Role of Quasiparticles in an Electric Circuit with Josephson Junctions

Benoît Rossignol, Thomas Kloss, and Xavier Waintal
University of Grenoble Alpes, CEA, INAC-Pheliqs, 38000 Grenoble, France

(Received 17 January 2019; published 22 May 2019)

Although Josephson junctions can be viewed as highly nonlinear impedances for superconducting quantum technologies, they also possess internal dynamics that may strongly affect their behavior. Here, we construct a computational framework that includes a microscopic description of the junction (full fledged treatment of both the superconducting condensate and the quasiparticles) in the presence of a surrounding electrical circuit. Our approach generalizes the standard resistor capacitor Josephson model to arbitrary junctions (including, e.g., multiterminal geometries and/or junctions that embed topological or magnetic elements) and arbitrary electric circuits treated at the classical level. By treating the superconducting condensate and quasiparticles on equal footings, we capture nonequilibrium phenomena such as multiple Andreev reflection. We show that the interplay between the quasiparticle dynamics and the electrical environment leads to the emergence of new phenomena. In a *RC* circuit connected to single channel Josephson junction, we find out-of-equilibrium current-phase relations that are strongly distorted with respect to the (almost sinusoidal) equilibrium one, revealing the presence of the high harmonic ac Josephson effect. In an *RLC* circuit connected to a junction, we find that the shape of the resonance is strongly modified by the quasiparticle dynamics: close to resonance, the current can be smaller than without the resonator. Our approach provides a route for the quantitative modeling of superconducting-based circuits.

DOI: 10.1103/PhysRevLett.122.207702

There is currently a huge effort around the world—both within academia and major industrial partners—to promote the superconducting transmon quantum bit [1–3] from a laboratory object to a viable technology for building a quantum computer. The central element of this approach is a weak normal link between two pieces of superconductors: the Josephson junction. Although tunneling junctions with an insulating (oxide) barrier are the most mature elements, other types of junctions such as atomic contacts [4] (with very few propagating channels), semiconducting nanowires [5] (with high spin-orbit suitable for stabilizing Majorana bound states), superconducting-ferromagnetic-superconducting [6,7] (with anomalous current-phase relations), or multiterminal devices [8] could provide new functionalities to the superconducting toolbox. Although the theoretical description of these objects is rather well understood [9], many relevant regimes lie outside of what may be treated analytically, and the development of numerical methods is important. In fact, the complexity of the circuits that are being created is increasing very rapidly, and building predictive numerical tools is a key element for the success of any quantum technology.

Two very successful complementary viewpoints are commonly used to describe Josephson junction circuits. The first one is the resistor capacitor Josephson (RCJ) model [10,11] that views the Josephson junction as a highly nonlinear impedance embedded in an electric circuit. In this model, one considers a classical circuit such as the ones shown in the insets of Fig. 1 or Fig. 3 with resistances ($V = RI$), capacitances ($I = C\partial_t V$), inductances ($V = L\partial_t I$) or other classical elements. The Josephson junction is described by its current-phase relation $I = I_c \sin\varphi$ and the Josephson relation $\partial_t\varphi = (2e/\hbar)V$.

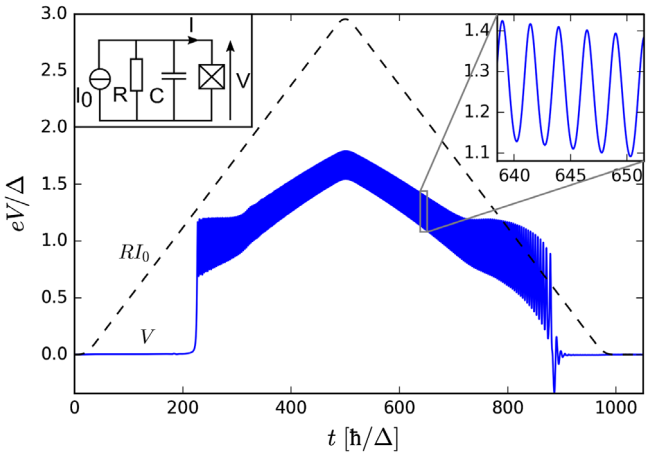

FIG. 1. Upper-left inset: simulated circuit, with an *RC* biased Josephson junction. Main panel: result of the *RC*-BdG simulation. Dashed line: voltage RI_0 applied by the generator versus time t. I_0 is raised and decreased slowly to keep the system quasiadiabatic. Blue line: voltage $V(t)$ measured across the junction. Upper-right inset: enlarged view of main curve revealing the oscillations due to the ac Josephson effect.

Such a simple model is surprisingly powerful. It captures the hysteresis loops of the I-V curves. Its simple extension, where one adds a Langevin stochastic term to account for finite temperature, accurately describes the noise properties found experimentally, including the probability for the junction to switch from the superconducting branch [12]. It has also been successfully used for more elaborate circuits that include resonators [13]. Its quantum extension provides the model used to design the various sorts of superconducting qubits [14] and has been shown to describe very accurately a large corpus of experimental data [15]. Yet, the model fails dramatically in some very simple limits. For instance, at large voltages, it does not properly reproduce the ohmic behavior of the circuit because the latter involves the excitation spectrum of the junction, which is not accounted for in the current-phase relation. More importantly, it does not account for some important out-of-equilibrium phenomena, such as multiple Andreev reflection (MAR) [16,17] processes.

The second model uses a microscopic mean-field description of the junction through the (time-dependent) Bogoliubov–De Gennes (BdG) equation. BdG models capture most of the salient features of these junctions, including those that contain exotic (e.g., topological or magnetic) materials. It naturally describes MAR [17], the interplay with microwaves [18], ac Josephson effects, and emergent topological effects in multiterminal geometries [19]. Until recently, however, the direct numerical integration of BdG equations has been very limited due to the intrinsic computational complexity [20] and did not include the electromagnetic environment of the junction.

The present Letter builds on recent advances made in time-dependent computational transport [21] to construct a numerical method that merges the RCJ model with the BdG equation, thereby providing a fully self-consistent treatment of the Josephson junction and its electromagnetic environment at the BdG level (hereafter called the RC-BdG model). The method has an arbitrary precision and is scalable to hundreds of thousands of orbitals, paving the way to the simulations of complex superconducting circuits. It applies to arbitrary BdG equations and classical electromagnetic environments.

Problem formulation.—We model our circuits in two parts. First, the junction itself is described with a microscopic BdG Hamiltonian $\hat{H}(\varphi, t)$ that depends explicitly on time t (through, e.g., a capacitive gate) and on the phase difference $\varphi(t)$ between the two superconductors (which extends to a vector when more than two superconductors are involved). Note that, due to the ac Josephson effect, the problem is intrinsically time dependent, even in the absence of time-dependent perturbations. Integrating the BdG equation provides the density matrix $\hat{\rho}(t)$ from which one can compute the current $I(t)$ that flows through the system. Below, we restrict ourself to the average current, but its quantum fluctuations are also accessible through our formalism [22]. The second part of the model describes the classical circuit, or the electromagnetic environment, that surrounds the junction. The classical equations that describe these circuits take the form of a differential equation for φ. More complex circuits are described in a similar way with more degrees of freedom describing the classical circuit. The set of equations reads

$$i\hbar\partial_t\hat{\rho} = [\hat{H}(\varphi, t), \hat{\rho}], \tag{1a}$$

$$I(t) = \mathrm{Tr}(\hat{I}\,\hat{\rho}), \tag{1b}$$

$$\frac{d^2\varphi}{dt^2} = F\left(\varphi, \frac{d\varphi}{dt}, I(t)\right), \tag{1c}$$

where the function $F(\varphi, d\varphi/dt, I(t))$ describes the dynamics of the classical circuit (RC or RLC equation in the examples below) with $I(t)$ as an external source term. We numerically solve the BdG equation within the Keldysh formalism using the approach developed in [23,24], where the problem is unfolded onto a set of Schrödinger equations for scattering wave functions. An efficient algorithm has been constructed in [20] to integrate the corresponding equations. The corresponding software, "T-KWANT," relies on the KWANT package [25] and will be released as open source in the near future. Equation (1) alone amounts to solving a few hundred time-dependent Schrödinger equations (with the actual number depending on the required energy resolution). The self-consistent condition [Eqs. (1b) and (1c)] makes the problem significantly more challenging because it creates nonlinear couplings between these Schrödinger equations. Following [21], we address this nonlinear coupling by taking advantage of the separation of timescales in the problem between the microscopic timescales of the BdG equation (which imposes discretized time steps of lengths much smaller than $\hbar/E_F$, with E_F as the Fermi energy) and the evolution of the electromagnetic variables $I(t)$ and $\varphi(t)$ that takes place on much slower timescales (typically gigahertz frequencies as compared with petahertz for the Fermi energy in actual devices). Hence, we use a doubly adaptive predictor-corrector approach for $\varphi(t)$ as explained in [21]: Eq. (1a) is integrated with a "predicted" function $\varphi(t)$, and Eqs. (1b) and (1c) are used on the larger timescale to construct this prediction. A straightforward time adaptive fourth order Runge-Kutta [26] is used for the integration of Eq. (1c). We used the algorithm of [27] to calculate the (Andreev) bound states of the model with precision. The method is general to any Hamiltonian $\hat{H}$ that is quadratic in creation and destruction operators. Hence, it may handle electron-electron interaction effects at the mean field level or random phase approximation level [21] but does not capture correlation effects. Static or dynamic disorder may be added directly [23]. The full code used for generating the data of this Letter can be found in [28].

To be specific, we now turn to a particular BdG Hamiltonian that describes a single channel junction. The BdG Hamiltonian describes a one-dimensional system with the two superconductors corresponding to $x < 0$ and $x > 0$, whereas the normal region is formed by a single site at $x = 0$, placing the system in the short junction limit,

$$\hat{H} = \sum_{\substack{x=-\infty \\ \sigma=\uparrow,\downarrow}}^{+\infty} e^{i\varphi(t)\delta_{x,-1}} \hat{c}^{\dagger}_{x\sigma}\hat{c}_{x+1,\sigma} + (U\delta_{x,0} - E_F)\hat{c}^{\dagger}_{x\sigma}\hat{c}_{x\sigma} + \sum_{x=-\infty}^{+\infty} \Delta(1-\delta_{x,0})\hat{c}^{\dagger}_{x\uparrow}\hat{c}^{\dagger}_{x\downarrow} + \text{H.c.} \quad (2)$$

Here, $\varphi(t) = (e/\hbar)\int^t V(t')dt'$, where $V(t)$ is the voltage difference across the junction, Δ is the superconducting gap inside the superconductors, and U is a potential barrier used to tune the transmission probability D of the junction. In the calculations below, we use $E_F = 2$, $\Delta = 0.1$ (which will be used as our unit of energy), and $U = 2$, which corresponds to a junction with an intermediate transmission of $D = 0.5$. For this value, the equilibrium current-phase relation has small deviations with respect to a sinusoidal shape, but the I-V characteristics of the isolated junction exhibit distinct cusps at voltages of $eV = \Delta/n$, $n \in \{1, 2, 3, \ldots\}$ (MAR) [17]. The precise relation $I(\varphi) = I_c \sin(\varphi)$ is recovered in the tunneling regime $D \ll 1$, and $eV < \Delta$ with $I_c = 2e\Delta D/h$.

Results for the RC-BdG model.—The first electromagnetic environment we consider is a simple RC circuit as sketched in Fig. 1. The capacitance C typically accounts for the electron-electron interaction in the junction itself, whereas the resistance R accounts for the finite residual resistance in the whole circuit. This RC circuit is the minimum electromagnetic environment that must be considered. The RCJ model for this circuit (where the BdG equation is replaced by the current-phase relation) reads

$$\frac{d^2\varphi}{dt^2} + \frac{1}{Q}\frac{d\varphi}{dt} + \sin(\varphi) = \frac{I_0}{I_c}, \quad (3)$$

where the time t has been rescaled as $t \to \omega_0 t$. $\omega_0 = \sqrt{\hbar I_c/(2eC)}$ is the intrinsic frequency of the circuit for small oscillating amplitudes, and $Q = RC\omega_0$ is the corresponding quality factor. The physics of this model is well understood [11]: for $I_0 < I_c$, all the current passes through the junction (supercurrent branch); whereas for $I_0 > I_c$, the equilibrium solution is unstable and a voltage develops across the junction. Interestingly, this model is hysteretic for underdamped circuits $Q > 1$, and a dynamical solution with $\dot{\varphi} \neq 0$ exists for some values of $I_0 < I_c$. At a high bias current $I_0 \gg I_c$, most of the current is dissipated by the resistor R, and the RCJ model predicts $I_0 = R\bar{V}$ (where $\bar{V}$ is the average voltage difference seen by the junction). This prediction misses an important contribution from the junction: its intrinsic resistance $R_J = h/(2e^2D)$ in the normal state. Indeed, at a large bias current, one expects $I_0 = (1/R + 1/R_J)\bar{V}$.

We now turn to the full simulation of the RC-BdG model. The bare simulation data are shown in Fig. 1, where the dashed line corresponds to a slow (quasistatic) ramp of I_0 so that the entire I-V characteristics of the device can be extracted from a single simulation. We ramp the current first up and then down to zero in order to capture the hysteresis loop of the junction. The blue line corresponds to the voltage across the junction as a function of time. As shown in the inset, the blue line contains an important oscillating part that corresponds to the ac Josephson effect. From these data, we calculate the voltage $\bar{V}$ across the junction, averaged over a small time window (to get rid of the ac Josephson signal). Figure 2 shows the resulting plot of I_0 versus $\bar{V}$ (blue line). The dotted line corresponds to the various asymptotic of the RCJ model discussed above, whereas the dashed line corresponds to the pure BdG model in the absence of the electromagnetic environment. The pure BdG model displays the usual kinks characteristics of the opening of a new MAR channel [18]. The RC-BdG simulations reconcile the two limits: the pure MAR curve at high bias, and the supercurrent branch of the RCJ model at small bias. In the crossover between these two extreme limits, it provides the minimum model that

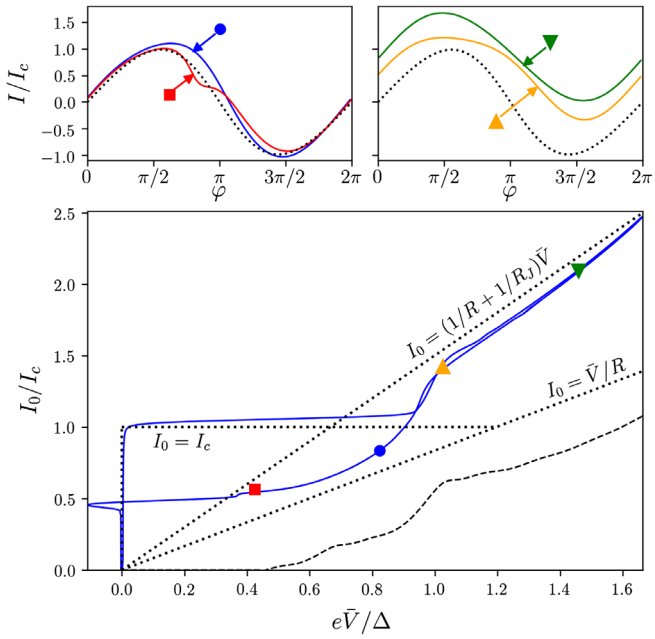

FIG. 2. RC-BdG model. Bottom panel: bias current I_0 versus the average voltage across the junction $\bar{V}$ for an underdamped oscillator $Q \approx 1.7$. Dotted lines: various asymptotes of the RCJ model; see text. Dashed line: pure BdG model without the environment. Upper panels: out-of-equilibrium current-phase relations at four different points of the $I_0 - \bar{V}$ curve. The dotted line corresponds to the equilibrium current-phase relation of the pure junction.

captures all important physical contributions, and hence quantitatively predicts the full hysteresis loop including the retrapping current. The most interesting features of the system show up in its dynamics. Recording the phase difference $\varphi(t)$ across the junction and the current $I(t)$ that flows through it, the dynamics is properly captured by the corresponding out-of-equilibrium current-phase I-φ relation obtained from the corresponding parametric plot. The result is shown in the upper panels of Fig. 2. Such out-of-equilibrium I-φ could be reconstructed from a high-frequency measurement of the different harmonic of $V(t)$. As a reference, Fig. 2 includes the equilibrium I-φ characteristics of the junction (dotted line) obtained by taking all contributions into account (i.e., both Andreev bound states and the small contribution from the continuous part of the spectrum). This equilibrium I-φ relation contains small deviations to the sinusoidal form. However, out-of-equilibrium relations can be strongly different from the simple sinusoidal shape. This is true in particular in the returning part of the hysteresis loop (red line, square, visible component of the second harmonic) and close to the MAR cusps (yellow line, triangle, strongly nonsinusoidal). In these regimes, the excursions in voltage across the junction are wide (as can be seen directly from Fig. 1) and the junction is effectively highly nonlinear.

Results for the RLC-BdG model.—We now turn to a second circuit where the junction is put in series with a classical RLC resonator, as sketched in the inset of Fig. 3. The electromagnetic circuit is slightly more complex than the previous RC model; but, in return, the highly nonlinear behavior shown in the previous example manifests itself already on dc observables. The resonator has a quality factor of $Q = R\sqrt{C/L}$ and a resonance pulsation of $\omega_0 = 1/\sqrt{LC}$. The corresponding impedance $Z(\omega)$ takes the form of $R/Z(\omega) = 1 + iQ[\omega/\omega_0 - \omega_0/\omega]$ and filters the frequency around ω_0. Such an environment has been studied in a series of recent experiments using tunnel junctions [29–32]. The RLC circuit provides a direct probe of the ac signal present in the system. We expect a main resonance for $2eV_J/\hbar = \omega_0$ when the ac Josephson effect drives the RLC circuit. Due to the nonlinear character of the junction, the higher harmonics of the ac Josephson effects are generated so that additional features are expected at $2eV_J/\hbar = \omega_0/n$. Likewise, the nonlinearities imply that the RLC circuit can also be driven parametrically at $2\omega_0$, leading to features at $eV_J/\hbar = \omega_0/n$.

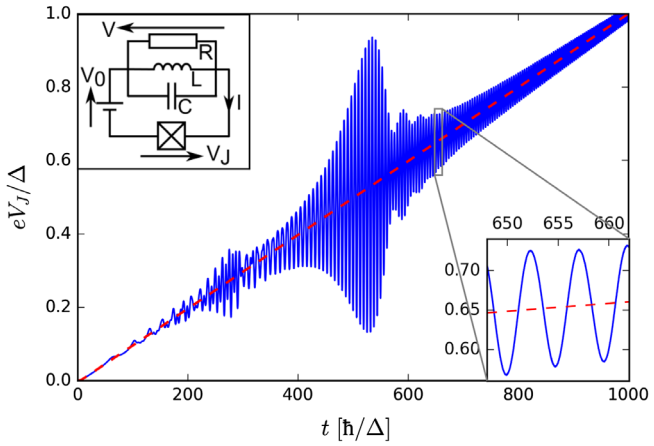

FIG. 3. RLC-BdG model. Upper inset: schematic of the RLC circuit. Main panel: voltage $V_J(t)$ across the junction (blue line) versus time t for a linear voltage ramp in $V_0(t)$ (red dashed line). $Q = 20$, $\omega_0 = \Delta$, and $R = 3h/2e^2 \simeq 38.7$ kΩ. Bottom inset: enlarged view of the main curve showing the ac Josephson effect oscillations. The resonance of the RLC circuit is visible for $eV_J = \hbar\omega_0/2$ and $eV_J = \hbar\omega_0/4$

We compare the RLC-BdG calculations with an improved RLCJ model. The improved RLCJ model captures the supercurrent branch and the MAR nonlinear I-V curve as

$$I(\varphi) = I_c \sin\varphi + I_{\mathrm{MAR}}(2e\dot{\varphi}/\hbar), \tag{4}$$

where $I_{\mathrm{MAR}}(V)$ is the dc nonlinear I-V characteristic of the junction in the absence of an electromagnetic environment (dashed line of Fig. 4). The numerical results for the average current $\bar{I}$ versus voltage are shown in Fig. 4 for four different RLC circuits with different frequencies ω_0. We concentrate on the main features around $2eV_J/\hbar = \omega_0$ and disregard the smaller peaks associated with higher harmonics and/or parametric pumping. The improved RLCJ model (dotted line) presents a Lorentzian-like resonance at $2eV_J/\hbar = \omega_0$ for all four RLC circuits. When the resonance lies in the tunneling regime of the junction (blue line), there is a very good agreement between the improved RLCJ model and the full RLC-BdG simulations. The agreement is also qualitatively (but not quantitatively) good when the resonance corresponds to high voltages in the almost "ohmic" regime of the junction (yellow line). However, for the two circuits where the resonance lies in

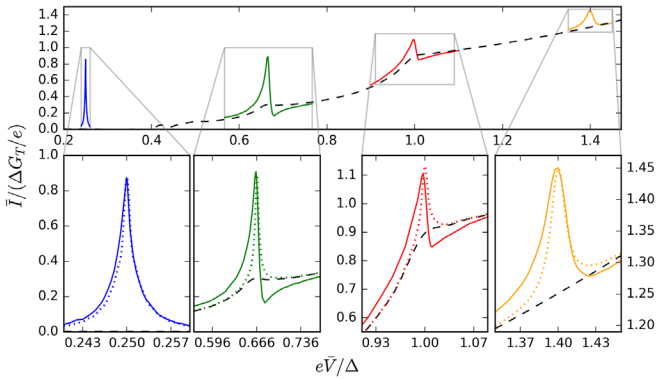

FIG. 4. Current-voltage relation for four different resonator frequencies $\omega_0/\Delta = 1/4, 2/3, 1$, and 1.4. Dashed line: $I_{\mathrm{MAR}}(V)$ in the absence of environment. Thin color lines: RLC-BdG simulations. Dotted lines: improved RLCJ model. Bottom panels: enlarged views of the main figure.

the vicinity of a kink of the $I_{\mathrm{MAR}}(V)$ characteristic, the two models are strikingly different and the improved RLCJ model is no longer applicable (green and red lines): the improved RLCJ model is typically off by $\pm 50\%$, including in the linewidth. In these regimes, we find that, for $2eV_J/\hbar > \omega_0$, the current is reduced with respect to $I_{\mathrm{MAR}}(V)$ instead of the Lorentzian increase observed in the improved RLCJ model. This reduction of the current is a direct manifestation of the nonlinear ac physics happening in the device. This dc prediction is the counterpart of the highly nonsinusoidal nonequilibrium current-phase relations discussed above for the RC-BdG case. However, the fact that the observable is in dc makes this prediction more easily accessible to an experimental test.

Conclusion.—The environment-BdG model presented in this Letter unifies simple RCJ-like models with microscopic models that include the quasiparticle spectrum of the junctions as well as its dynamics out of equilibrium. We have shown that the interplay between the two physics strongly modifies the behavior of the system and leads to new phenomena, such as the voltage induced nonsinusoidal current-phase relations. Our approach provides a practical route to study the engineering of electromagnetic environments in the presence of junctions that go beyond simple tunneling devices. Besides the example studied in this Letter (a single channel junction with arbitrary transparency), other systems such as Josephson field effect transistors [33], Majorana devices [34], and multiterminal devices [35] that are being developed by the community could be studied with the same technique [36]. On the technical level, the approach could be extended to include electron-electron interaction and/or a self-consistent calculation of the superconducting gap at the time-dependent mean-field level [21].

This work was supported by ANR Fully Quantum (Project No. ANR-16-CE30-0015-02), ANR QTERA (Project No. ANR-15-CE24-0007-02), NSF-ANR partnership PIRE: HYBRID, and the U.S. Office of Naval Research. We thank Manuel Houzet and Julia Meyer for useful discussions.

[1] J. Koch, T. M. Yu, J. Gambetta, A. A. Houck, D. I. Schuster, J. Majer, A. Blais, M. H. Devoret, S. M. Girvin, and R. J. Schoelkopf, Charge-insensitive qubit design derived from the cooper pair box, Phys. Rev. A **76**, 042319 (2007).

[2] R. Barends, J. Kelly, A. Megrant, D. Sank, E. Jeffrey, Y. Chen, Y. Yin, B. Chiaro, J. Mutus, C. Neill, P. O'Malley, P. Roushan, J. Wenner, T. C. White, A. N. Cleland, and J. M. Martinis, Coherent Josephson Qubit Suitable for Scalable Quantum Integrated Circuits, Phys. Rev. Lett. **111**, 080502 (2013).

[3] H. Paik, D. I. Schuster, L. S. Bishop, G. Kirchmair, G. Catelani, A. P. Sears, B. R. Johnson, M. J. Reagor, L. Frunzio, L. I. Glazman, S. M. Girvin, M. H. Devoret, and R. J. Schoelkopf, Observation of High Coherence in Josephson Junction Qubits Measured in a Three-Dimensional Circuit QED Architecture, Phys. Rev. Lett. **107**, 240501 (2011).

[4] M. F. Goffman, R. Cron, A. Levy Yeyati, P. Joyez, M. H. Devoret, D. Esteve, and C. Urbina, Supercurrent in Atomic Point Contacts and Andreev States, Phys. Rev. Lett. **85**, 170 (2000).

[5] V. Mourik, K. Zuo, S. M. Frolov, S. R. Plissard, E. P. A. M. Bakkers, and L. P. Kouwenhoven, Signatures of Majorana fermions in hybrid superconductor-semiconductor nanowire devices, Science **336**, 1003 (2012).

[6] Y. A. Izyumov, Y. N. Proshin, and M. G. Khusainov, Competition between superconductivity and magnetism in ferromagnet-superconductor heterostructures, Usp. Fiz. Nauk **172**, 113 (2002).

[7] A. I. Buzdin, Proximity effects in superconductor-ferromagnet heterostructures, Rev. Mod. Phys. **77**, 935 (2005).

[8] R.-P. Riwar, M. Houzet, J. S. Meyer, and Y. V. Nazarov, Multi-terminal Josephson junctions as topological matter, Nat. Commun. **7**, 11167 (2016).

[9] A. A. Golubov, M. Y. Kupriyanov, and E. Il'ichev, The current-phase relation in Josephson junctions, Rev. Mod. Phys. **76**, 411 (2004).

[10] K. K. Likharev, Superconducting weak links, Rev. Mod. Phys. **51**, 101 (1979).

[11] W. C. Stewart, Current-voltage characteristics of Josephson junctions, Appl. Phys. Lett. **12**, 277 (1968).

[12] E. Ben-Jacob, D. J. Bergman, B. J. Matkowsky, and Z. Schuss, Lifetime of oscillatory steady states, Phys. Rev. A **26**, 2805 (1982).

[13] M. C. Cassidy, A. Bruno, S. Rubbert, M. Irfan, J. Kammhuber, R. N. Schouten, A. R. Akhmerov, and L. P. Kouwenhoven, Demonstration of an ac Josephson junction laser, Science **355**, 939 (2017).

[14] Z.-L. Xiang, S. Ashhab, J. Q. You, and F. Nori, Hybrid quantum circuits: Superconducting circuits interacting with other quantum systems, Rev. Mod. Phys. **85**, 623 (2013).

[15] M. H. Devoret, D. Esteve, H. Grabert, G.-L. Ingold, H. Pothier, and C. Urbina, Effect of the Electromagnetic Environment on the Coulomb Blockade in Ultrasmall Tunnel Junctions, Phys. Rev. Lett. **64**, 1824 (1990).

[16] T. Klapwijk, G. Blonder, and M. Tinkham, Explanation of subharmonic energy gap structure in superconducting contacts, Physica (Amsterdam) **109–110(B+C)**, 1657 (1982).

[17] D. Averin and A. Bardas, ac Josephson Effect in a Single Quantum Channel, Phys. Rev. Lett. **75**, 1831 (1995).

[18] J. C. Cuevas, J. Heurich, A. Martín-Rodero, A. Levy Yeyati, and G. Schön, Subharmonic Shapiro Steps and Assisted Tunneling in Superconducting Point Contacts, Phys. Rev. Lett. **88**, 157001 (2002).

[19] M. Houzet, J. S. Meyer, D. M. Badiane, and L. I. Glazman, Dynamics of Majorana States in a Topological Josephson Junction, Phys. Rev. Lett. **111**, 046401 (2013).

[20] J. Weston and X. Waintal, Linear-scaling source-sink algorithm for simulating time-resolved quantum transport and superconductivity, Phys. Rev. B **93**, 134506 (2016).

[21] T. Kloss, J. Weston, and X. Waintal, Transient and Sharvin resistances of luttinger liquids, Phys. Rev. B **97**, 165134 (2018).

[22] B. Gaury and X. Waintal, A computational approach to quantum noise in time-dependent nanoelectronic devices, Physica (Amsterdam) **75E**, 72 (2016).

[23] B. Gaury, J. Weston, M. Santin, M. Houzet, C. Groth, and X. Waintal, Numerical simulations of time-resolved quantum electronics, Phys. Rep. **534**, 1 (2014).

[24] J. Weston and X. Waintal, Towards realistic time-resolved simulations of quantum devices, J. Comput. Electron. **15**, 1148 (2016).

[25] C. W. Groth, M. Wimmer, A. R. Akhmerov, and X. Waintal, Kwant: A software package for quantum transport, New J. Phys. **16**, 063065 (2014).

[26] E. Hairer, G. Wanner, and S. P. Norsett, *Solving Ordinary Differential Equations I* (Springer, Berlin, 1993).

[27] M. Istas, C. Groth, A. Akhmerov, M. Wimmer, and X. Waintal, A general algorithm for computing bound states in infinite tight-binding systems, SciPost Phys. **4**, 026 (2018).

[28] B. Rossignol, K. Thomas, J. Weston, B. Gaury, C. Groth, and X. Waintal, Role of the quasi-particles in an electric circuit with Josephson junctions (code and data) (2019), https://doi.org/10.5281/zenodo.2585908.

[29] M. Westig, B. Kubala, O. Parlavecchio, Y. Mukharsky, C. Altimiras, P. Joyez, D. Vion, P. Roche, D. Esteve, M. Hofheinz, M. Trif, P. Simon, J. Ankerhold, and F. Portier, Emission of Nonclassical Radiation by Inelastic Cooper Pair Tunneling, Phys. Rev. Lett. **119**, 137001 (2017).

[30] R. W. Simmonds, K. M. Lang, D. A. Hite, S. Nam, D. P. Pappas, and J. M. Martinis, Decoherence in Josephson Phase Qubits from Junction Resonators, Phys. Rev. Lett. **93**, 077003 (2004).

[31] M. Reagor, W. Pfaff, C. Axline, R. W. Heeres, N. Ofek, K. Sliwa, E. Holland, C. Wang, J. Blumoff, K. Chou, M. J. Hatridge, L. Frunzio, M. H. Devoret, L. Jiang, and R. J. Schoelkopf, Quantum memory with millisecond coherence in circuit QED, Phys. Rev. B **94**, 014506 (2016).

[32] V. Zaretskey, B. Suri, S. Novikov, F. C. Wellstood, and B. S. Palmer, Spectroscopy of a cooper-pair box coupled to a two-level system via charge and critical current, Phys. Rev. B **87**, 174522 (2013).

[33] T. Akazaki, H. Takayanagi, J. Nitta, and T. Enoki, A Josephson field effect transistor using an InAs-inserted-channel $In_{0.52}Al_{0.48}As/In_{0.53}Ga_{0.47}As$ inverted modulation-doped structure, Appl. Phys. Lett. **68**, 418 (1996).

[34] S. D. Sarma, M. Freedman, and C. Nayak, Majorana zero modes and topological quantum computation, npj Quantum Inf. **1**, 15001 (2015).

[35] A. N. McCaughan and K. K. Berggren, A superconducting-nanowire three-terminal electrothermal device, Nano Lett. **14**, 5748 (2014).

[36] J. Weston, B. Gaury, and X. Waintal, Manipulating Andreev and Majorana bound states with microwaves, Phys. Rev. B **92**, 020513(R) (2015).